catalysts

MDPI

Article

Reactor Design for CO_2 Photo-Hydrogenation toward Solar Fuels under Ambient Temperature and Pressure

Chun-Ying Chen [1], Joseph Che-Chin Yu [1], Van-Huy Nguyen [2], Jeffrey Chi-Sheng Wu [1,*], Wei-Hon Wang [3] and Kamila Kočí [4]

1 Department of Chemical Engineering, National Taiwan University, Taipei 10617, Taiwan; r01541131@ntu.edu.tw (C.-Y.C.); d03524016@ntu.edu.tw (J.C.-C.Y.)
2 Faculty of Chemical and Environmental Engineering, Lac Hong University, 812431, No. 10 Huynh Van Nghe, Buu Long, Bien Hoa, Dong Nai, Viet Nam; d10106811@mail.ntust.edu.tw
3 Chung-Shan Institute of Science and Technology, Tao Yuan 32599, Taiwan; cubic.wang@msa.hinet.net
4 Institute of Environmental Technology, VŠB-Technical University of Ostrava, 17. listopadu 15/2172, 708 33 Ostrava-Poruba, Czech Republic; kamila.koci@vsb.cz
* Correspondence: cswu@ntu.edu.tw; Tel.: +886-2-23631994; Fax: +886-2-23623040

Academic Editor: Rajendra S. Ghadwal
Received: 27 December 2016; Accepted: 8 February 2017; Published: 16 February 2017

Abstract: Photo-hydrogenation of carbon dioxide (CO_2) is a green and promising technology and has received much attention recently. This technique could convert solar energy under ambient temperature and pressure into desirable and sustainable solar fuels, such as methanol (CH_3OH), methane (CH_4), and formic acid (HCOOH). It is worthwhile to mention that this direction can not only potentially depress atmospheric CO_2, but also weaken dependence on fossil fuel. Herein, 1 wt % $Pt/CuAlGaO_4$ photocatalyst was successfully synthesized and fully characterized by ultraviolet-visible light (UV-vis) spectroscopy, X-ray diffraction (XRD), Field emission scanning electron microscopy using energy dispersive spectroscopy analysis (FE-SEM/EDS), transmission electron microscopy (TEM), X-ray photoelectron spectroscopy (XPS), and Brunauer-Emmett-Teller (BET), respectively. Three kinds of experimental photo-hydrogenation of CO_2 in the gas phase, liquid phase, and gas-liquid phase, correspondingly, were conducted under different H_2 partial pressures. The remarkable result has been observed in the gas-liquid phase. Additionally, increasing the partial pressure of H_2 would enhance the yield of product. However, when an extra amount of H_2 is supplied, it might compete with CO_2 for occupying the active sites, resulting in a negative effect on CO_2 photo-hydrogenation. For liquid and gas-liquid phases, CH_3OH is the major product. Maximum total hydrocarbons 8.302 $\mu mol \cdot g^{-1}$ is achieved in the gas-liquid phase.

Keywords: CO_2 reduction; $Pt/CuAlGaO_4$; photo-hydrogenation; photocatalysis; solar fuels

1. Introduction

Nowadays, it is important to develop an efficient and effective method for utilizing carbon dioxide (CO_2) greenhouse gas. The CO_2 captured from the atmosphere will be stored in the ground or the ocean [1]. Another option, which is a more attractive method for CO_2 consumption, is to convert it into useful hydrocarbon fuels directly [2]. In industry, CO_2 is widely used for Sabatier reaction [3,4] and reverse water-gas shift (RWGS) reaction [5,6]. Regarding the Sabatier reaction, CO_2 reacts with H_2 to form CH_4 and H_2O at 300–400 °C. As for RWGS reaction, CO_2 firstly reacts with H_2 to form CO and H_2O; then CO can be easily converted into hydrocarbons by the Fischer-Tropsch reaction. However, both reactions require high temperature and high pressure to reduce CO_2 into hydrocarbons. Thus, it is inevitable to develop another method to conduct CO_2 reduction.

The possible CO_2 conversion processes, including biological [7], catalytic [8–11], photocatalytic [12–14], and electrocatalytic [15,16] conversion are summarized in Table 1. Among these processes, photocatalytic CO_2 reduction is one of the most promising technologies and has received much attention recently [14,17–21]. CO_2 as a C1-feedstock could be reduced to desirable and sustainable solar fuels at ambient conditions under light irradiation.

Table 1. Summary of different processes of CO_2 reduction.

Conversion Process	Main Products	Advantages	Disadvantages	Ref.
Biological	HCOOH: conversion efficiency of $(22 \pm 9) \times 10^{-2}$%	Biological capability to synthesize liquid fuels	Complicated and cumbersome biological processes	[7]
Catalytic (Heterogeneous catalysis)	CH_4: 3.8×10^4 μmol·h^{-1}·g^{-1} catalyst CH_3OH: 8.8% of CO_2 conversion with the corresponded selectivity of 63% CH_3OH: 193.9 g·kg_{cat}^{-1}·h^{-1}	High efficiency	High temperature requirement	[8] [9] [10]
Catalytic (Homogeneous catalysis)	CH_3OH: 79% yield			[11]
Photocatalytic (Heterogeneous catalysis)	CH_4: 0.56 μmol h^{-1}·g^{-1} catalyst CH_3OH: 4.6 μmol h^{-1}·g^{-1} catalyst	Storage of solar energy	Low efficiency	[12] [13]
Photocatalytic (Homogeneous catalysis)	CO: 12.66 h^{-1} of TOF			[14]
Electrocatalytic	Liquid fuels	Converting CO_2 directly to liquid fuels (long-chain molecule)	High energy barrier needs overcoming	[15,16]

Ideally, photocatalytic CO_2 reduction could provide an alternative and sustainable pathway to producing desired hydrocarbon products from renewable energy and CO_2. However, it is noted that their efficiency is still relatively low. To enhance the photocatalytic performances, several factors—such as light harvesting, loss of photons, product separation, and charge carrier recombination—are considered in our group to design and developed in a new photo-reactor. In 2007, a circulated photocatalytic reactor was developed, which could provide a large specific surface area and uniformity of gas concentrations in the reactor [22]. In 2008, the optical-fiber photo-reactor, which could deliver light efficiently and uniformly to the surface of a photocatalyst, was also successfully designed [23]. It is important to note that there are two main sources to conduct CO_2 reduction, $H_2O_{(g)}$ and $H_{2(g)}$. In a previous study, Abbott et al. calculated a series of changes of enthalpy (ΔH^0) and changes of Gibbs free energy (ΔG^0), respectively, for CO_2 reduction to form hydrocarbons [24]. The result clearly shows that adding H_2 largely decreases these values. That is, the CO_2 reducing reaction in which the involved H_2 requires lower energy and becomes more spontaneous. Therefore, in 2013, a novel twin reactor was successfully developed to hydrogenate CO_2 into CH_3OH [20]. However, it is noted that its efficiency is still relatively low.

In this study, 1 wt % $Pt/CuAlGaO_4$ was prepared using a well-known solid-state fusion and photo-deposition method, respectively. Detailed characterization of photocatalyst was conducted to reveal its structure. Three kinds of reactors—including gas phase reactor, liquid phase reactor, and gas-liquid reactor—were designed and employed to study the influence of hydrogen (H_2) and carbon dioxide (CO_2) on the photo-hydrogenation of CO_2. Additionally, a possible reaction pathway of CO_2 photo-hydrogenation is also proposed based on the knowledge of products presented during the photocatalytic reaction.

2. Results and Discussion

2.1. Characterization of Photocatalysts

All photocatalysts were fully characterized by several techniques. Brunauer-Emmett-Teller (BET), ultraviolet-visible light (UV-vis) spectroscopy; X-ray diffraction (XRD), transmission electron microscopy (TEM), and Field emission scanning electron microscopy (FE-SEM) using energy dispersive spectroscopy (EDS) analysis were used to reveal their structure and surface morphology

of photocatalysts. X-ray photoelectron spectroscopy (XPS) was used to reveal the chemical state of the species.

Figure 1 displays the UV-vis light absorption spectra of $CuAlGaO_4$ and 1 wt % $Pt/CuAlGaO_4$ photocatalysts, respectively. Clearly, all the photocatalysts have the absorption band in the range of 250–670 nm, which is consistent with that reported previously [25]. It notes that loading of the Pt neither significantly improves the light absorption nor changes the band gap. A possible reason comes from the fact that Pt loading is very small and highly dispersed on the supporting surface.

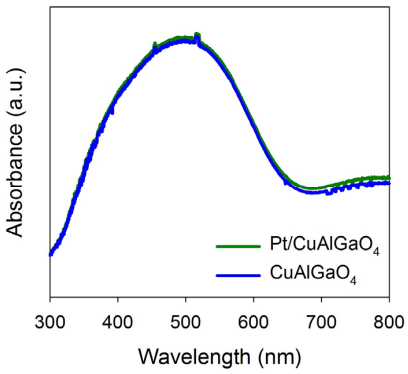

Figure 1. Ultraviolet-visible light (UV-vis) spectra for $CuAlGaO_4$ and 1 wt % $Pt/CuAlGaO_4$ photocatalysts.

Figure 2 shows the XRD patterns of $CuAlGaO_4$, 1 wt % $Pt/CuAlGaO_4$ photocatalysts and their starting materials of CuO, Al_2O_3, and Ga_2O_3. Clearly, no peaks can be assigned to either CuO, Al_2O_3, or Ga_2O_3, indicating that complete reaction of the precursors was achieved by solid-state fusion a mixture of Al_2O_3, Ga_2O_3, and ZnO at 1125 K for 12 h. The loading of Pt obviously retains the structural features of $CuAlGaO_4$ photocatalyst, but its crystallites appear to be slightly decreased. Both photocatalysts have patterns similar to that of the single-phase spinel type structure of the $CuAlGaO_4$ (JCPDS file, card No. 26-0514). However, there is no noticeable crystalline phase observed in the XRD pattern of $Pt/CuAlGaO_4$ photocatalyst that can be attributed to Pt element. As discussed above, the Pt loading might be very small and highly dispersed on the supporting surface, which is consistent with the UV-vis spectrum.

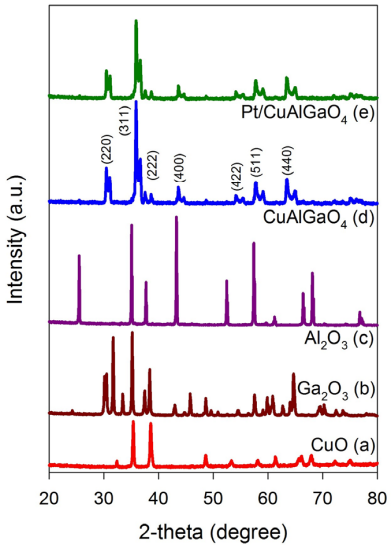

Figure 2. X-ray diffraction (XRD) patterns of photocatalysts: $CuAlGaO_4$ and 1 wt % $Pt/CuAlGaO_4$, in compared with starting materials of CuO, Al_2O_3, and Ga_2O_3.

Figure 3 shows the SEM images with corresponded elemental spectra of $CuAlGaO_4$ and 1 wt % $Pt/CuAlGaO_4$ photocatalysts, respectively. For $CuAlGaO_4$ photocatalyst, it has cube-like particles and smooth surfaces. Most importantly, loading of Pt on $CuAlGaO_4$ could not change the shape and morphology of the photocatalyst. Additionally, a uniform distribution of the Pt particles was found with a narrow size range of 4–20 nm.

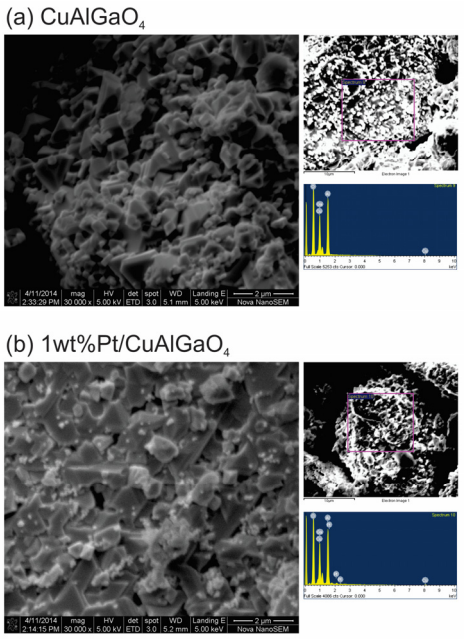

Figure 3. Scanning electron microscopy (SEM) images with corresponded elemental spectra of (**a**) $CuAlGaO_4$ and (**b**) 1 wt % $Pt/CuAlGaO_4$ photocatalysts.

Table 2 shows elemental analysis of $CuAlGaO_4$ and 1 wt % $Pt/CuAlGaO_4$, respectively. It clearly points out that only 1 wt % $Pt/CuAlGaO_4$ showed the Pt signal (Figure 3). On the other hand, the other elemental signals (O, Al, Cu, Ga) were very similar between $CuAlGaO_4$ and 1 wt % $Pt/CuAlGaO_4$ photocatalysts.

Table 2. Energy dispersive spectroscopy (EDS) analysis for element compositions of $CuAlGaO_4$ and 1 wt % $Pt/CuAlGaO_4$ photocatalysts.

Element	Atomic Ratio (%)	
	$CuAlGaO_4$	**$Pt/CuAlGaO_4$**
O	61.9	61.6
Al	23.0	22.0
Cu	12.8	13.0
Ga	2.3	3.2
Pt	N/D [1]	0.2

[1] N/D—Not detection.

Figure 4 reveals the TEM images, which were conducted to further understand the presenting of Pt loading on 1 wt % $Pt/CuAlGaO_4$ photocatalyst. It has several well-dispersed Pt nanoparticles with corresponded size of near 4–20 nm are located on the surface of $Pt/CuAlGaO_4$ photocatalyst.

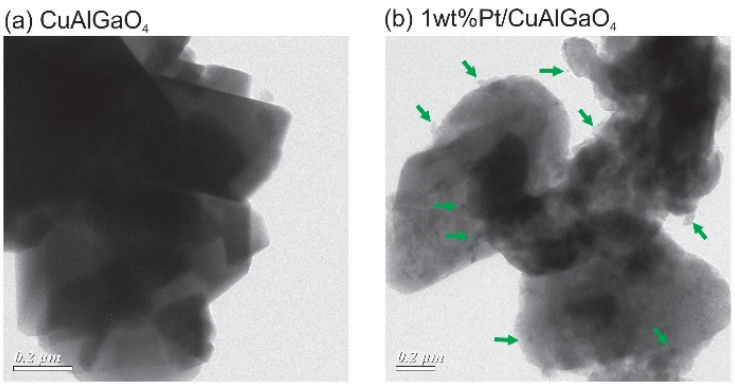

Figure 4. Transmission electron microscopy (TEM) images of photocatalysts: (**a**) $CuAlGaO_4$ and (**b**) 1 wt % $Pt/CuAlGaO_4$ photocatalysts.

XPS Pt4f spectra of $CuAlGaO_4$ and 1 wt %$Pt/CuAlGaO_4$ photocatalysts are shown in Figure 5. Most importantly, there are two possible peaks at 73.6–74.1 and 77.0–77.4 eV have been observed for 1 wt % $Pt/CuAlGaO_4$ photocatalyst, which may be attributed to $4f_{7/2}$ and $4f_{5/2}$ of Pt oxide, respectively [26].

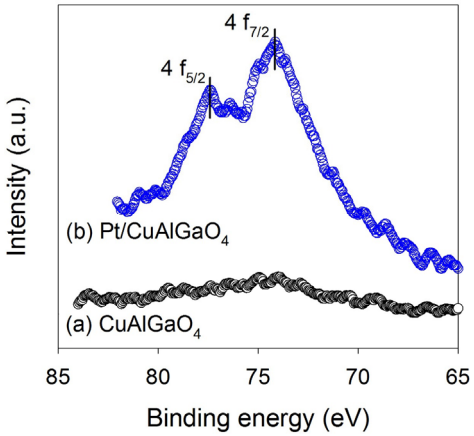

Figure 5. The Pt 4f X-ray photoelectron spectroscopy (XPS) spectra for (**a**) $CuAlGaO_4$ and (**b**) 1 wt % $Pt/CuAlGaO_4$ photocatalysts.

Lastly, the BET surface area of $CuAlGaO_4$ and 1 wt % $Pt/CuAlGaO_4$ was approximately 0.65 and 0.86 $m^2 \cdot g^{-1}$, respectively. Both values were not very high due to the solid-state fusion method which operates at a high temperature, causing the photocatalyst aggregation.

2.2. Photocatalytic CO_2 Reduction with Gas, Liquid, Gas-Liquid Phase Reactors

In this study, several blank tests in all type of reactors (gas phase, liquid phase, and gas-liquid phase reactors) were conducted to answer the question whether the formation of the reaction products come from photo-hydrogenation and not from CO_2 contaminations or the photocatalyst itself. The result of tests was shown in Table 3. The result clearly shows that if CO_2 was not introduced to the reacting system, no product was generated even with the presence of the hydrogen, photocatalyst, and light irradiation. It is important to remember that the photocatalyst synthesis process did not use any carbon-containing precursor. This blank test result is further confirmation that the photocatalyst itself contains nearly no carbon residue. Table 3 also clearly shows that, without any of three essential elements in performing the photo-hydrogenation reaction, including (a) CO_2, (b) photocatalyst and (c) light source, no product could be detected.

Table 3. Summary of blank tests for photo-hydrogenation of CO_2.

No.	Type of Reactors	Experimental Conditions				Yield of Products ($\mu mol \cdot g^{-1}$)
		CO_2	H_2 (0.01 atm)	Photocatalyst (1 wt % $Pt/CuAlGaO_4$)	Light Source	
1	Gas phase reactor	X [1]	O [2]	O	O	BDL [3]
2		O	O	X	O	BDL
3		O	O	O	X	BDL
4	Liquid phase reactor	X	O	O	O	BDL
5		O	O	X	O	BDL
6		O	O	O	X	BDL
7	Gas-liquid phase reactor	X	O	O	O	BDL
8		O	O	X	O	BDL
9		O	O	O	X	BDL

[1] X—absent in the photoreactor; [2] O—present in the photoreactor; [3] BDL—below the detection limit of gas chromatography.

For CO_2 reduction, there are several possible C_1 products, such as formic acid, formaldehyde, methanol, and methane. Because of the high detection limit of formaldehyde by HPLC (3.3 ppm), we used the Nash reagent [27] to react with formaldehyde first, then analyzed the colored product diacetyldihydrolutidine (DDL) by UV-vis at 414 nm to quantify the formaldehyde. The detail was described in the previous literature [27,28]. Even the detection limit of this method was 0.17 $\mu mol \cdot L^{-1}$, which was about three orders lower than HPLC, formaldehyde was not observed under all investigated conditions. However, it is noted that although we did not detect formaldehyde, some of the formaldehyde might also be formed on the surface of the catalyst [29,30]. For the gas phase reactor, there is also no formic acid and methanol could be detected, and only methane evolution would be discussed in this case. The CH_4 yield under gas phase conditions was shown in Figure 6.

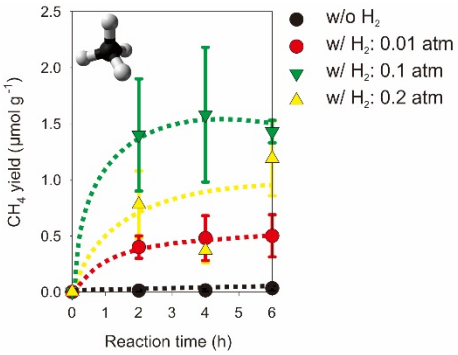

Figure 6. The time-dependent yield of CH_4 evolution over 1 wt % $Pt/CuAlGaO_4$ photocatalyst under different $H_{2(g)}$ partial pressures in a gas phase reactor. Lines are not based on a kinetic model and are presented for eye-guiding only.

Most interestingly, H_2 plays an active role on CH_4 yield.

$$CO_{2(g)} + 4H_{2(g)} \rightarrow CH_{4\,(g)} + 2H_2O_{(l)}$$
$$\Delta H^0 = -259.9\ kJ/mol;\ \Delta G^0 = -132.4\ kJ/mol \quad (1)$$

It is evident that the conversion of CO_2 into CH_4 has negative ΔH^0 and ΔG values, meaning that the process is spontaneous, equilibrium favorable, and exothermic. In this study, the enthalpy (ΔH^0) and Gibbs free energy (ΔG^0) values at 298 K for several interesting reactions were calculated by Aspen [31]. At first 2 h, the initial rates of CH_4 yield were 0.01, 0.57, 0.73, and 0.40 $\mu mol \cdot g^{-1} \cdot h^{-1}$ that

correspond to H_2 partial pressure = 0, 0.01, 0.1, 0.2 atm, respectively. It is worth noting that increasing the partial pressure of H_2 would enhance the yield of the product. Among the conditions of H_2 partial pressure, 0.1 atm shows the best performance. However, an extra supply of H_2 might compete with CO_2 for occupying the active sites, bringing a negative effect on CO_2 photo-hydrogenation. As shown in Figure 6, CH_4 evolution became stable after two hours in reaction, implying that the reactions in the system reached a dynamic equilibrium.

A comparative experiment was also conducted in the liquid phase. The correlation between the amount of CH_4, CH_3OH, and HCOOH formed and the reaction time for the liquid phase are shown in Figure 7.

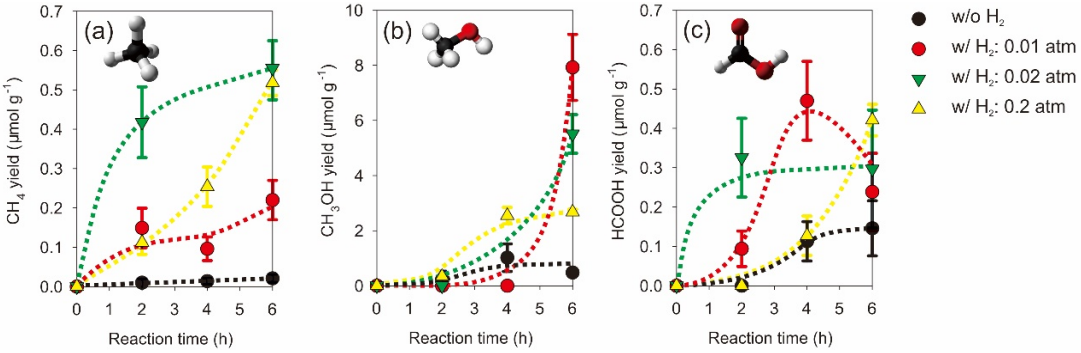

Figure 7. The time-dependent yield of (**a**) CH_4 evolution, (**b**) CH_3OH formation, and (**c**) HCOOH formation over 1 wt % $Pt/CuAlGaO_4$ photocatalyst under different $H_{2(g)}$ partial pressures in a liquid phase reactor. Lines are not based on a kinetic model and are presented for eye-guiding only.

The main products of the liquid phase reactor were CH_4, CH_3OH, and HCOOH, respectively.

$$\begin{gathered} CO_{2(g)} + 3H_{2(g)} \rightarrow CH_3OH_{(l)} + H_2O_{(l)} \\ \Delta H^0 = -137.8\ \text{kJ/mol};\ \Delta G^0 = -10.7\ \text{kJ/mol} \end{gathered} \tag{2}$$

$$\begin{gathered} CO_{2(g)} + H_{2(g)} \rightarrow HCOOH_{(l)} \\ \Delta H^0 = -31.0\ \text{kJ/mol};\ \Delta G^0 = +34.3\ \text{kJ/mol} \end{gathered} \tag{3}$$

It is clear that all exothermic reactions exhibit negative ΔH^0 values. Moreover, many reactions are also associated with negative ΔG^0 values and, as a consequence, the reaction will be thermodynamically favorable. Most importantly, CH_3OH was found to be the major product under current condition. This fact is that CH_3OH requires only six photoelectrons for the photo-hydrogenation of CO_2 while CH_4 needs to have eight photoelectrons for reaction. Last but not least, an extra amount of H_2 provided may also suppress the yield of products, which is consistent with the observation in the gas phase.

The correlations between the amount of CH_4, CH_3OH, and HCOOH formed and the reaction time for the combined gas-liquid phase are shown in Figure 8.

Similar to the result of the liquid phase, CH_3OH still is the main product for gas-liquid phase. On the other hand, the CH_4 yield has a tendency to be suppressed after conducting the experiment for two hours. It is possible that an intermediate product of CO_2 photo-reduction, CO, could be generated as the reaction proceeds (Equation (4)). Following is the competing reaction pathways of photo-reduction of CO to CH_3OH and HCOOH via H_2 and H_2O, respectively (Equations (5) and (6)). This result implies that the presence of photocatalyst in the gas phase will promote the converting of CH_4 into another compound, such as CH_3OH or HCOOH, resulting in a decrease of CH_4 yield.

$$\begin{gathered} CO_{2(g)} + CH_{4(g)} \rightarrow 2CO_{(g)} + 2H_{2(g)} \\ \Delta H^0 = -247.5\ \text{kJ/mol};\ \Delta G^0 = +170.8\ \text{kJ/mol} \end{gathered} \tag{4}$$

$$CO_{(g)} + 2H_{2(g)} \rightarrow CH_3OH_{(l)}$$
$$\Delta H^0 = -131.6 \text{ kJ/mol}; \Delta G^0 = -29.9 \text{ kJ/mol} \quad (5)$$

$$CO_{(g)} + H_2O_{(g)} \rightarrow HCOOH_{(l)}$$
$$\Delta H^0 = -24.8 \text{ kJ/mol}; \Delta G^0 = +15.1 \text{ kJ/mol} \quad (6)$$

In brief summary, the possible reaction pathways of CO_2 photo-hydrogenation is illustrated in Scheme 1. This mechanism is proposed based on the knowledge of products presented during the photocatalytic reaction. Our observation indicates that CH_4 is the only product under gas phase condition. On the other hand, CH_4, CH_3OH, and HCOOH are found in the liquid and gas-liquid phase reactions. Although we could not measure an intermediate CO product quantitatively, we expect that CO might be generated during the reaction. In the gas-liquid phase reactor, the photocatalyst is well packed and dispersed on the quartz plate in the gas phase. Hence, it might promote the transformation of CO into CH_3OH and HCOOH products. We do believe that conducting the experiment in different phases (such as gas, liquid, and gas-liquid phases) could not change the mechanism of the photo-hydrogenation of CO_2. However, the presence of photocatalyst in different phases might accelerate different pathways of the reaction.

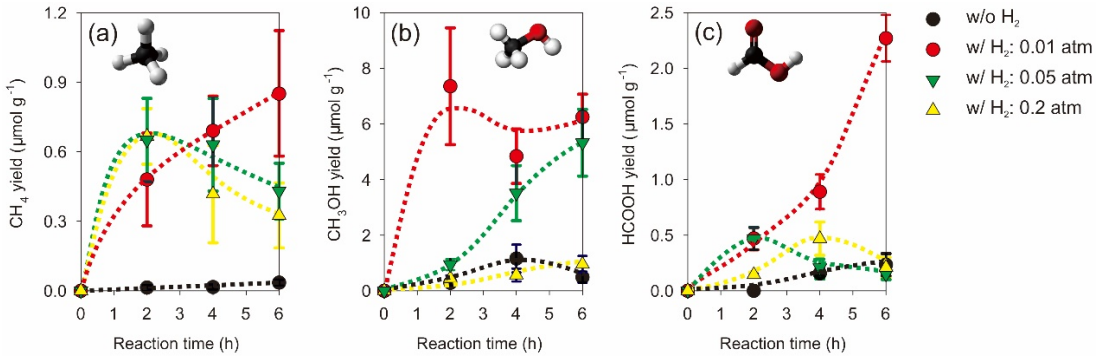

Figure 8. The time-dependent yield of (**a**) CH_4 evolution, (**b**) CH_3OH formation, and (**c**) HCOOH formation over 1 wt % $Pt/CuAlGaO_4$ photocatalyst under different $H_{2(g)}$ partial pressures in gas-liquid phase reactor. Lines are not based on a kinetic model and are presented for eye-guiding only.

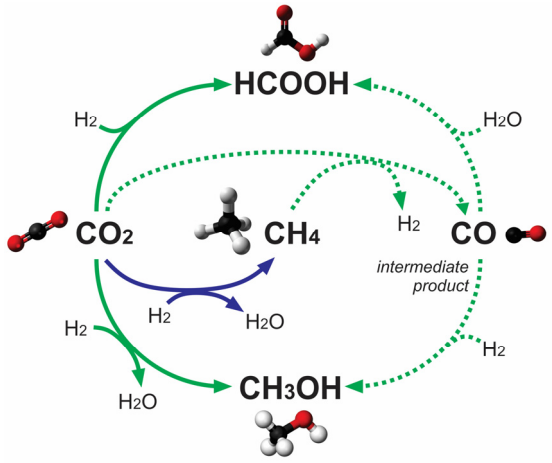

Scheme 1. The reaction pathways during the photo-hydrogenation of CO_2.

Table 4 summarizes the product yields at two hours in three kinds of reactors under different H_2 partial pressures. We see that H_2 plays an active role in the photocatalytic reduction of CO_2. Additionally, a remarkable synergetic activity was clearly observed when the experiment was conducted in gas-liquid phase under 0.01 atm of H_2. In more detail, the total products in the gas

and liquid phase are 0.400 and 0.243 μmol·g^{-1}, respectively. Interestingly, about 8.302 μmol·g^{-1} is achieved in the gas-liquid phase.

Table 4. Summary of the product yields at 2 h in three kinds of reactors over 1 wt % Pt/$CuAlGaO_4$ under different H_2 partial pressures.

Entry	Phase	H_2 Partial Pressure (atm)	Product Yields (μmol·g^{-1})			
			CH_4	CH_3OH	HCOOH	Total HCs [1]
1	Gas	0.00	0.012 ± 0.010	BDL [2]	BDL	0.012
2		0.01	0.400 ± 0.100	BDL	BDL	0.400
3		0.20	0.780 ± 0.300	BDL	BDL	0.780
4	Liquid	0.00	0.010 ± 0.010	0.235 ± 0.100	BDL	0.245
5		0.01	0.149 ± 0.050	BDL	0.094 ± 0.045	0.243
6		0.20	0.112 ± 0.030	0.340 ± 0.200	BDL	0.452
7	Gas-Liquid	0.00	0.014 ± 0.010	0.285 ± 0.100	BDL	0.299
8		0.01	0.480 ± 0.200	7.352 ± 2.100	0.470 ± 0.100	8.302
9		0.20	0.666 ± 0.120	0.445 ± 0.110	0.145 ± 0.010	1.255

[1] Total hydrocarbons yield = CH_4 yield + CH_3OH yield + HCOOH yield); [2] BDL—below the detection limit of gas chromatography.

Lastly, the quantum efficiencies in three kinds of reactors under 0.01 atm of H_2 are also calculated. The highest quantum efficiency was in the gas-liquid phase reactor for 0.0011%, while the gas and liquid phases were about 0.0001% and 0.0005%, respectively. The possible reason for higher quantum efficiency in the gas-liquid phase reactor is that both H_2 in the gas phase and the proton in liquid phase could be utilized simultaneously, affording more chances to conduct CO_2 photo-reduction.

3. Materials and Methods

3.1. Preparation of Photocatalysts

$CuAlGaO_4$ photocatalyst was firstly prepared by solid-state fusion method, which is mentioned in previous studies [19,25]. Firstly, copper oxide (CuO, Showa, Tokyo, Japan), aluminum oxide (Al_2O_3, Type A-5, Sigma-Aldrich, St. Louis, MO, USA), and β-gallium trioxide (β-Ga_2O_3, ≥99.9%, Sigma-Aldrich) powders were mixed in the molar ratio of Cu/Al/Ga = 1:1:1 and pulverized in a mortar. Subsequently, the resulting mixture was calcined at 1150 °C for 12 h, and then cooled to room temperature and further pulverized to obtain a $CuAlGaO_4$ powder.

1 wt % Pt/$CuAlGaO_4$ photocatalyst was prepared by the photo-deposition method as described in the same reference. The required amount of chloroplatinic acid hydrate ($H_2PtCl_6 \cdot xH_2O$, ≥99.9%, Sigma-Aldrich) solution was mixed with the as-prepared $CuAlGaO_4$ powder. Herein, the loading of Pt on $CuAlGaO_4$ is 1 wt %. The mixed solution was irradiated by a UV source (320–500 nm, EXFO S1500, EXFO Inc., Quebec City, QC, Canada) for 90 min to perform the photo-deposition process. After that, the solid product was centrifuged and washed with deionized water several times. Finally, the washed material was dried at 80 °C for 8 h to obtain 1 wt % Pt/$CuAlGaO_4$ powder.

3.2. Characterization of Photocatalysts

X-ray diffractometer (XRD, Ultima IV, Rigaku, Tokyo, Japan) equipped with Cu Kα (1.5418 Å) was used to verify the crystalline structure of photocatalysts. The UV-vis diffuse reflectance spectrum of the photocatalyst was fully recorded over the range 300–800 nm by a Cary 100 UV-visible spectrometer (UV-vis, Varian Cary 100, Agilent Technologies, Santa Clara, CA, USA). $BaSO_4$ was used as the reflectance standard. A field emission scanning electron microscope (FE-SEM, Nano SEM 230, FEI, Hillsboro, OR, USA) equipped with energy dispersive spectroscopy (EDS) was used to directly reveal the presence of the atomic elements in the photocatalysts. Transmission electron microscopy

(TEM, Hitachi H-7100, Hitachi Inc., Tokyo, Japan) was performed to check the surface morphology of $CuAlGaO_4$ and 1 wt % $Pt/CuAlGaO_4$. The state of Pt loaded on $CuAlGaO_4$ was determined by X-ray photoelectron spectroscopy (XPS, Thermo Theta Probe, Thermo Fisher Scientific Inc., East Grinstead, UK) equipped with a Mg Kα (1253.6 eV) X-ray source. The Brunauer-Emmett-Teller (BET) surface area of photocatalysts was measured by a specific surface area analyzer (ASAP 2020, Micromeritics, Norcross, GA, USA).

3.3. Photo-Hydrogenation of CO_2 Reaction

In this study, we perform the experiments in three kinds of batch reactor systems: gas phase reactor, liquid phase reactor, and the gas-liquid phase reactor (Scheme 2).

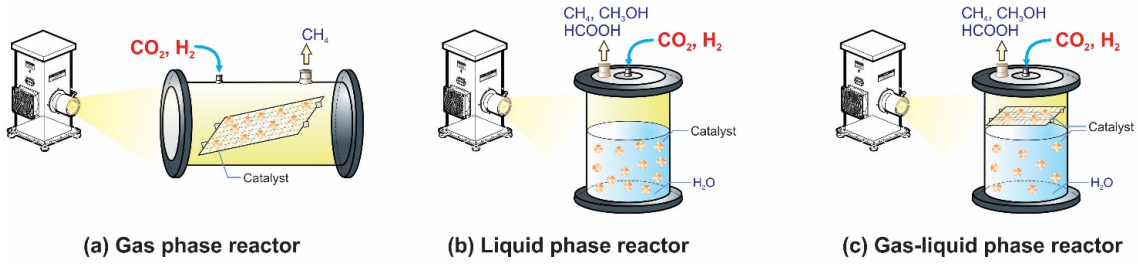

Scheme 2. Three kinds of reactors: (**a**) Gas phase reactor; (**b**) liquid phase reactor; (**c**) gas-liquid phase reactor.

For the gas phase reactor, the cylindrical tube reactor was made of Pyrex with a volume of 260 mL (Scheme 2a). A quartz plate, 92 × 40 × 2 mm, was placed inside the reactor and inclined at an angle of 20° to face the light source, 300 W Xenon lamp (Model 66902, Newport, Irvine, CA, USA). During the photoreaction, the light source was placed at an equal-distance from the reactor to the lamp so that the catalyst could receive the same amount of light intensity (mostly visible light), which was around 270 $mW \cdot cm^{-2}$. Powder photocatalyst (0.30 g) was evenly packed on the quartz plate. For the liquid phase reactor, the reactor was also made by Pyrex with a volume of 385 mL (Scheme 2b). 0.30 g photocatalyst was well dispersed in the liquid phase with stirring. A 300 W Xenon lamp was also provided as the light source. The liquid phase solution, which contained 180 mL 0.1 M NaOH (Alfa Aesar, Ward Hill, MA, USA), was used to increase the solubility of CO_2. For the gas-liquid phase reactor (Scheme 2c), it was almost the same with the liquid phase reactor that combined with a Teflon plate. 0.10 g and 0.20 g 1 wt % $Pt/CuAlGaO_4$ photocatalysts were well packed and dispersed on the Teflon plate and in the solution, respectively. Before introducing the CO_2 (99.999%, Air Products, Taipei, Taiwan) and H_2 (99.99%, Air Products) into the reactor, Argon (99.9995%, Air Products) was purged to bring out any impurity contained within.

In this study, all the samples were taken and analyzed every two hours. Both methane (CH_4, gas phase) and methanol (CH_3OH, liquid phase) were detected by individual GC-FID (China GC 2000, China Chromatography Co., Taipei, Taiwan) equipped with a packed column (molecular sieve 5A, 3.5 m) with a carrier gas of Ar (99.9995%, Air Products). Formic acid (HCOOH, liquid phase) was detected by High Performance Liquid Chromatography (HPLC) (Shodex RI-2000, Shoko Co., Tokyo, Japan) equipped with a column (ICSep ICE-ORH-801, 300 mm, Interchim, Montluçon, France).

4. Conclusions

A potentially clean, low-cost CO_2 photo-hydrogenation method to convert the solar energy into desirable and sustainable energy—such as methanol, methane, and formic acid—has been demonstrated. In this study, CO_2 as a C1-feedstock was photo-reduced in the gas phase, liquid phase, and gas-liquid phase, respectively, over 1 wt % $Pt/CuAlGaO_4$ photocatalyst under different H_2 partial pressures. Interestingly, a remarkable result has been observed in the gas-liquid phase.

The result also shows that increasing the partial pressure of H_2 could improve the yield of products. However, it notes that H_2 might compete with CO_2 for occupying the active sites when an extra amount of H_2 is provided, bringing about the adverse effect on CO_2 photo-hydrogenation. For liquid and gas-liquid phases, CH_3OH is the major product while CH_4 is the only product for the gas phase. The quantum efficiencies in gas, liquid, and gas-liquid phase under 0.01 atm of H_2 are about 0.0001%, 0.0005%, and 0.0011%, respectively. It is worthwhile to mention that this direction not only can potentially depress atmospheric CO_2, but also weaken dependence on fossil fuel.

Acknowledgments: The authors gratefully acknowledge the Chung-Shan Institute of Science & Technology, Taiwan (Grant No. CSIST-808-V309(103)), and the Ministry of Science and Technology, Taiwan (Grant No. NSC 103-2923-E-002-009-MY3), and Grant Agency of the Czech Republic (project No. 14-35327J) for financial support.

Author Contributions: Jeffrey Chi-Sheng Wu, Chun-Ying Chen, and Wei-Hon Wang conceived and designed the experiments; Chun-Ying Chen performed the experiments; Chun-Ying Chen, Van-Huy Nguyen, and Joseph Che-Chin Yu analyzed the data; Van-Huy Nguyen and Joseph Che-Chin Yu wrote the paper. Wei-Hon Wang and Kamila Kočí participated in research discussion.

Conflicts of Interest: The authors declare no conflict of interest.

References

1. Yang, H.; Xu, Z.; Fan, M.; Gupta, R.; Slimane, R.B.; Bland, A.E.; Wright, I. Progress in carbon dioxide separation and capture: A review. *J. Environ. Sci.* **2008**, *20*, 14–27. [CrossRef]
2. Roy, S.C.; Varghese, O.K.; Paulose, M.; Grimes, C.A. Toward solar fuels: Photocatalytic conversion of carbon dioxide to hydrocarbons. *ACS Nano* **2010**, *4*, 1259–1278. [CrossRef] [PubMed]
3. Lunde, P.J.; Kester, F.L. Rates of methane formation from carbon dioxide and hydrogen over a ruthenium catalyst. *J. Catal.* **1973**, *30*, 423–429. [CrossRef]
4. Thampi, K.R.; Kiwi, J.; Gratzel, M. Methanation and photo-methanation of carbon dioxide at room temperature and atmospheric pressure. *Nature* **1987**, *327*, 506–508. [CrossRef]
5. Daza, Y.A.; Kent, R.A.; Yung, M.M.; Kuhn, J.N. Carbon dioxide conversion by reverse water-gas shift chemical looping on perovskite-type oxides. *Ind. Eng. Chem. Res.* **2014**, *53*, 5828–5837. [CrossRef]
6. Bustamante, F.; Enick, R.M.; Cugini, A.V.; Killmeyer, R.P.; Howard, B.H.; Rothenberger, K.S.; Ciocco, M.V.; Morreale, B.D.; Chattopadhyay, S.; Shi, S. High-temperature kinetics of the homogeneous reverse water-gas shift reaction. *AIChE J.* **2004**, *50*, 1028–1041. [CrossRef]
7. Noji, T.; Jin, T.; Nango, M.; Kamiya, N.; Amao, Y. CO_2 photoreduction by formate dehydrogenase and a Ru-complex in a nanoporous glass reactor. *ACS Appl. Mater. Interfaces* **2017**, *9*, 3260–3265. [CrossRef]
8. Abe, T.; Tanizawa, M.; Watanabe, K.; Taguchi, A. CO_2 methanation property of Ru nanoparticle-loaded TiO_2 prepared by a polygonal barrel-sputtering method. *Energy Environ. Sci.* **2009**, *2*, 315–321. [CrossRef]
9. Liu, X.; Song, Y.; Geng, W.; Li, H.; Xiao, L.; Wu, W. Cu-Mo_2C/MCM-41: An efficient catalyst for the selective synthesis of methanol from CO_2. *Catalysts* **2016**, *6*, 75. [CrossRef]
10. Huang, C.; Chen, S.; Fei, X.; Liu, D.; Zhang, Y. Catalytic hydrogenation of CO_2 to methanol: Study of synergistic effect on adsorption properties of CO_2 and H_2 in CuO/ZnO/ZrO_2 system. *Catalysts* **2015**, *5*, 1846. [CrossRef]
11. Kothandaraman, J.; Goeppert, A.; Czaun, M.; Olah, G.A.; Prakash, G.K.S. Conversion of CO_2 from air into methanol using a polyamine and a homogeneous ruthenium catalyst. *J. Am. Chem. Soc.* **2016**, *138*, 778–781. [CrossRef] [PubMed]
12. Yui, T.; Kan, A.; Saitoh, C.; Koike, K.; Ibusuki, T.; Ishitani, O. Photochemical reduction of CO_2 using TiO_2: Effects of organic adsorbates on TiO_2 and deposition of Pd onto TiO_2. *ACS Appl. Mater. Interfaces* **2011**, *3*, 2594–2600. [CrossRef] [PubMed]
13. Li, X.; Wang, Q.; Zhao, Y.; Wu, W.; Chen, J.; Meng, H. Green synthesis and photo-catalytic performances for ZnO-reduced graphene oxide nanocomposites. *J. Colloid Interface Sci.* **2013**, *411*, 69–75. [CrossRef] [PubMed]
14. Cui, S.-C.; Sun, X.-Z.; Liu, J.-G. Photo-reduction of CO_2 using a rhenium complex covalently supported on a graphene/TiO_2 composite. *ChemSusChem* **2016**, *9*, 1698–1703. [CrossRef] [PubMed]
15. Benson, E.E.; Kubiak, C.P.; Sathrum, A.J.; Smieja, J.M. Electrocatalytic and homogeneous approaches to conversion of CO_2 to liquid fuels. *Chem. Soc. Rev.* **2009**, *38*, 89–99. [CrossRef] [PubMed]

16. Rezaei, B.; Mokhtarianpour, M.; Ensafi, A.A.; Hadadzadeh, H.; Shakeri, J. Electrocatalytic reduction of CO_2 using the dinuclear rhenium(i) complex [$ReCl(CO)_3$(μ-tptzH)$Re(CO)_3$]. *Polyhedron* **2015**, *101*, 160–164. [CrossRef]
17. Inoue, T.; Fujishima, A.; Konishi, S.; Honda, K. Photoelectrocatalytic reduction of carbon dioxide in aqueous suspensions of semiconductor powders. *Nature* **1979**, *277*, 637–638. [CrossRef]
18. Sastre, F.; Puga, A.V.; Liu, L.; Corma, A.; García, H. Complete photocatalytic reduction of CO_2 to methane by H_2 under solar light irradiation. *J. Am. Chem. Soc.* **2014**, *136*, 6798–6801. [CrossRef] [PubMed]
19. Biswas, S.K.; Baeg, J.-O.; Kale, B.B.; Yadav, R.K.; Moon, S.-J.; Kong, K.-j.; So, W.-W. An efficient visible-light active photocatalyst $CuAlGaO_4$ for solar hydrogen production. *Catal. Commun.* **2011**, *12*, 651–654. [CrossRef]
20. Lee, W.-H.; Liao, C.-H.; Tsai, M.-F.; Huang, C.-W.; Wu, J.C.S. A novel twin reactor for CO_2 photoreduction to mimic artificial photosynthesis. *Appl. Catal. B* **2013**, *132–133*, 445–451. [CrossRef]
21. Li, K.; Peng, B.; Peng, T. Recent advances in heterogeneous photocatalytic CO_2 conversion to solar fuels. *ACS Catal.* **2016**, *6*, 7485–7527. [CrossRef]
22. Lo, C.-C.; Hung, C.-H.; Yuan, C.-S.; Wu, J.-F. Photoreduction of carbon dioxide with H_2 and H_2O over TiO_2 and ZrO_2 in a circulated photocatalytic reactor. *Sol. Energy Mater. Sol. Cells* **2007**, *91*, 1765–1774. [CrossRef]
23. Nguyen, T.-V.; Wu, J.C.S.; Chiou, C.-H. Photoreduction of CO_2 over ruthenium dye-sensitized TiO_2-based catalysts under concentrated natural sunlight. *Catal. Commun.* **2008**, *9*, 2073–2076. [CrossRef]
24. Abbott, M.M.; Smith, J.M.; Van Ness, H.C. *Introduction to Chemical Engineering Thermodynamics*; McGraw-Hill Book Co. InC.: Boston, MA, USA, 1949; pp. 619–626.
25. Cheng, Y.-H.; Nguyen, V.-H.; Chan, H.-Y.; Wu, J.C.S.; Wang, W.-H. Photo-enhanced hydrogenation of CO_2 to mimic photosynthesis by CO co-feed in a novel twin reactor. *Appl. Energy* **2015**, *147*, 318–324. [CrossRef]
26. Wagner, C.D.; Muilenberg, G.E. *Handbook of X-ray Photoelectron Spectroscopy: A Reference Book of Standard Data for Use in X-ray Photoelectron Spectroscopy*; Perkin-Elmer Corp., Physical Electronics Division: Eden Prairie, MN, USA, 1979; p. 190.
27. Nash, T. The colorimetric estimation of formaldehyde by means of the hantzsch reaction. *Biochem. J.* **1953**, *55*, 416–421. [CrossRef] [PubMed]
28. Hong, J.; Zhang, W.; Ren, J.; Xu, R. Photocatalytic reduction of CO_2: A brief review on product analysis and systematic methods. *Anal. Methods* **2013**, *5*, 1086–1097. [CrossRef]
29. Yang, C.-C.; Vernimmen, J.; Meynen, V.; Cool, P.; Mul, G. Mechanistic study of hydrocarbon formation in photocatalytic CO_2 reduction over Ti-SBA-15. *J. Catal.* **2011**, *284*, 1–8. [CrossRef]
30. Mei, B.; Pougin, A.; Strunk, J. Influence of photodeposited gold nanoparticles on the photocatalytic activity of titanate species in the reduction of CO_2 to hydrocarbons. *J. Catal.* **2013**, *306*, 184–189. [CrossRef]
31. Xu, X.; Moulijn, J.A. Mitigation of CO_2 by chemical conversion: Plausible chemical reactions and promising products. *Energy Fuels* **1996**, *10*, 305–325.